Current Optics and Photonics
Vol. 3, No. 1, February 2019, pp. 8-15

ISSN: 2508-7266(Print) / ISSN: 2508-7274(Online)
DOI: https://doi.org/10.3807/COPP.2019.3.1.008

Common Optical System for the Fusion of Three-dimensional Images and Infrared Images

Duck-Lae Kim*, Bo Hee Jung, Hyun-Bae Kong, Chang-Min Ok, and Seung-Tae Lee

Seeker & EO/IR R&D Lab, LIG Nex1, Yongin 16911, Korea

(Received October 13, 2018 : revised December 11, 2018 : accepted December 11, 2018)

We describe a common optical system that merges a LADAR system, which generates a point cloud, and a more traditional imaging system operating in the LWIR, which generates image data. The optimum diameter of the entrance pupil was determined by analysis of detection ranges of the LADAR sensor, and the result was applied to design a common optical system using LADAR sensors and LWIR sensors; the performance of these sensors was then evaluated. The minimum detectable signal of the 128 × 128-pixel LADAR detector was calculated as 20.5 nW. The detection range of the LADAR optical system was calculated to be 1,000 m, and according to the results, the optimum diameter of the entrance pupil was determined to be 15.7 cm. The modulation transfer function (MTF) in relation to the diffraction limit of the designed common optical system was analyzed and, according to the results, the MTF of the LADAR optical system was 98.8% at the spatial frequency of 5 cycles per millimeter, while that of the LWIR optical system was 92.4% at the spatial frequency of 29 cycles per millimeter. The detection, recognition, and identification distances of the LWIR optical system were determined to be 5.12, 2.82, and 1.96 km, respectively.

Keywords : Atmospheric turbulence, LIDAR, Thermal imaging, Optical design
OCIS codes : (010.1330) Atmospheric turbulence; (010.3640) Lidar; (040.6808) Thermal (uncooled) IR detectors, arrays and imaging; (220.2740) Geometric optical design

I. INTRODUCTION

Recently, there has been a need to develop a technology to obtain three-dimensional (3D) image information at high speeds, while processing and tracking image information in real time. 3D image sensors, which are a core component of LADAR (Laser Radar) systems, have been developed from single-pixel detectors to focal-plane arrays (FPAs). Because LADAR sensors have high spatial resolution and can provide high resolution, they have the advantage of enabling the identification of even hidden objects, by acquiring and processing 3D images in many directions [1-3]. LADAR sensors can be used in the application of LADAR to aviation [4]. LADAR systems are being developed for the acquisition and fusion of 3D LADAR images with 2D CCD camera images, or infrared camera images [5, 6]. Optical systems that use a combination of LADAR sensors, CCD sensors, and infrared sensors are being developed as common optical systems for high-speed operation and downsizing. LWIR (Long Wavelength Infrared) sensors are noncooling types, and have advantages for downsizing and weight reduction; moreover, target identification is possible day or night.

When optical systems using LADAR sensors are designed, the detection-range analysis should be considered first. The detection range is determined by the laser's output power, ambient conditions, and detector and optical-system specifications. The ambient conditions should be considered during system design, because they affect the detection range and laser pointing errors of the LADAR system. For a LADAR optical system, the optimum diameter of the entrance pupil can be determined by analyzing the detection range of the pupil, considering the operating conditions of the LADAR system. When a common optical system using both LADAR and infrared sensors is designed, the specifications for the LADAR

*Corresponding author: kimducklae@lignex1.com, ORCID 0000-0003-1321-0341
Color versions of one or more of the figures in this paper are available online.

camera should be determined first, because the target-detection performance of a LADAR camera is lower than that of an infrared camera. In particular, the entrance pupil of the LADAR optical system is a parameter that becomes a standard when a common optical system is designed.

In the present study, the LADAR detector was analyzed, to obtain the minimum detectable signal of the 3D-image-capturing LADAR detector; the refractive-index structure was calculated, to analyze the ambient conditions; and the detection range of the LADAR sensor was analyzed, to obtain the diameter of the entrance pupil of the LADAR optical system. Using the results of analysis and calculation, a common optical system using LADAR sensors and LWIR sensors was design and analyzed.

II. ATMOSPHERIC-CONDITION ANALYSIS

When a laser beam passes through the atmosphere, it is attenuated or its optical path changes depending on the atmospheric air conditions. The refractive-index structure function was analyzed, to determine changes in the path of the laser beam due to atmospheric air turbulence. The refractive-index structure function was obtained by analyzing the Hufnagel-Valley model and the Miller-Zieske model. The Hunfnagel-Valley model is expressed as a refractive-index structure function, as shown by the following formula [7].

$$C_n^2(h) = 5.94\times10^{-23}e^{-h}\left(\frac{W}{27}\right) + 2.7\times10^{-16}e^{-2h/3} + 1.7\times10^{-14}e^{-10h} \quad (1)$$

where h is the altitude and W is an adjustable wind correlating parameter of 21 [8].

The Miller-Zieske model is expressed as a refractive-index structure function for the daytime model Eq. (2) and the night model Eq. (3) as shown in the following formulas [9].

$$\begin{aligned} C_n^2(h) &= 1.7\times10^{-14} && 0<h<18.5 \text{ m}, \\ &= 3.13\times10^{-13}/h^{1.05} && 18.5<h<240 \text{ m}, \\ &= 1.3\times10^{-15} && 240<h<880 \text{ m}, \\ &= 8.87\times10^{-7}/h^{3} && 880<h<7{,}200 \text{ m}, \\ &= 2.0\times10^{-16}/h^{1/2} && 7{,}200<h<20{,}000 \text{ m}. \end{aligned} \quad (2)$$

$$\begin{aligned} C_n^2(h) &= 8.4\times10^{-15} && 0<h<18.5 \text{ m}, \\ &= 2.87\times10^{-12}/h^{2} && 18.5<h<110 \text{ m}, \\ &= 2.5\times10^{-16} && 110<h<1500 \text{ m}, \\ &= 8.87\times10^{-7}/h^{3} && 1{,}500<h<7{,}200 \text{ m}, \\ &= 2.0\times10^{-16}/h^{1/2} && 7{,}200<h<20{,}000 \text{ m}. \end{aligned} \quad (3)$$

where h represents the altitude.

Figure 1 shows the refractive-index structures for the atmospheric air models, for different altitudes. When the

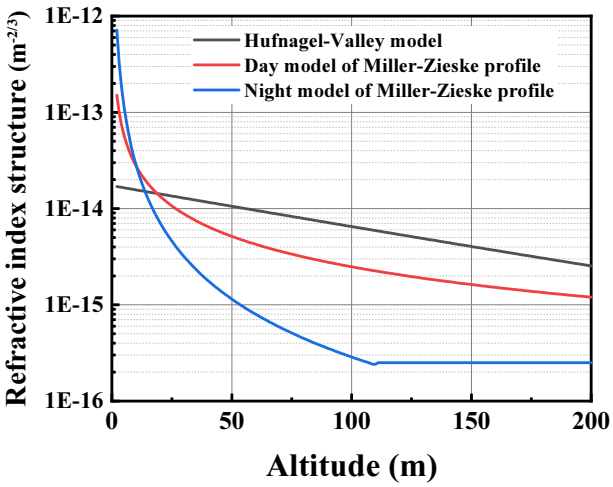

FIG. 1. Refractive-index structures for the atmospheric air models, in relation to the altitude.

LADAR sensor is used as a LADAR navigator, the effects of atmospheric air on the altitude must be considered. In general, the LADAR navigator has been reported to be operated at an altitude of 200 m [10] and a slant range of 1,000 m [11]. As shown in Fig. 1, the refractive-index structure shows a tendency to increase as the altitude decreases, which generates the beam-wander effect. When the laser beam penetrates the atmosphere, the optical path is affected by the beam-wander effect, so that the laser beam irradiates several points instead of one point on the target. At an altitude of 200 m, the refractive-index structure function was calculated as 2.54×10^{-15} $m^{-2/3}$ when the Hufnagel-Valley model was applied, and as 1.20×10^{-15} $m^{-2/3}$ and 2.5×10^{-16} $m^{-2/3}$ for daytime and nighttime in the Miller-Zieske model respectively. According to the literature, the refractive-index structure is divided according to atmospheric air conditions (turbulence strength) into 5×10^{-14} $m^{-2/3}$ under strong conditions, 1×10^{-14} 5×10^{-15} $m^{-2/3}$ under moderate conditions, and 1×10^{-15} $m^{-2/3}$ or lower under weak conditions. When calculating the detection range, the refractive-index structure was set to 5×10^{-15} $m^{-2/3}$, considering the calculated values and the literature [12].

III. LADAR SENSOR DETECTION-RANGE ANALYSIS

Detectors intended to satisfy the required performance of LADAR basically use linear-mode avalanche photodiodes (LMAPD) or Geiger-mode avalanche photodiodes (GMAPD) [13]. The LMAPD operates at a bias voltage that is lower than the breakdown voltage, and is used together with a current-amplifying stage. The GMAPD is used at a bias voltage that is *not* lower than the breakdown voltage, and can detect weak signals at the level of a single photon; however, it has a characteristic of responding to photons

TABLE 1. LADAR sensor specification

Parameter	Units	Value
Spectral range	μm	1.55
Pixel format	pixels	128 × 128
Pitch	μm	100
Responsivity @ M = 10	A/W	6.1
Dark current @ M = 10	nA	<25
Bandwidth @ M = 10	GHz	6.2

only once during the detection time. Applying the GMAPD in LADAR systems is advantageous in securing the maximum detection-range performance, because its photon sensitivity is higher than that of the LMAPD. However, it is vulnerable to various types of noise, and cannot easily distinguish materials based on reflectivity, because it measures only the time to return after being reflected. The LMAPD has strong noise characteristics, plus the advantage of relatively easy image implementation, because it can measure the pulse shape and intensity of the laser being reflected [14]. In the present study, the performance specification of the OptoGration Co.'s (In,Ga)As-(In,Al)As -based LMAPD was applied, to consider laser wavelengths and enhance the detected target tracking performance. The LADAR detector specification is provided in Table 1. The detector can amplify signals 10 times at a voltage of 0.55 V; in this case, the responsivity is 6.1 A/W, and the dark current is not higher than 25 nA. The noise-equivalent power (NEP) is 4.1 nW. When the threshold value for recognition of laser signals as pulses by the system is assumed to be five times the noise-equivalent power, to stably detect the laser signals reflected by the target, the minimum detectable signal at the LADAR system applied with the detector is calculated as 20.5 nW. The applied specification is a result of fabrication of 100 pixels per cm^2, and lower dark-current specifications are expected to be implemented when APD sensors with 128 × 128 pixels and 100 μm pitch are fabricated.

To determine the parameters for the design of a common optical system, the detection range of the LADAR sensor should be evaluated. As the pulsed laser beam generated by the laser light source passes through the atmospheric air, its peak output power is reduced. The laser beam incident on the target is reflected only partially, depending on the size of the target and the angle of incidence and reflectivity of the laser beam. Out of the reflected laser beam, only the quantity of light corresponding to the size of the entrance pupil of the LADAR optical system is received by the LADAR sensor. The LADAR sensor processes signals only when laser signals exceeding several times the circuit noise have been received, and recognizes the target thereafter through the algorithm. The detection range can be calculated using Eq. (4) [15].

$$P_{Rx}=\left(\frac{E_{Pulse}}{\Delta t}\tau_{Tx}\right)\left(e^{-\alpha_1 R_1}\right)\rho\cos\theta\int_{-\frac{H}{2}}^{\frac{H}{2}}\int_{-\frac{W}{2}}^{\frac{W}{2}}\frac{\exp\left(-\frac{(x-u_{BS})^2}{2R_1^2\left(\delta_b^2+\delta_j^2+\left(\frac{3.98\left(\frac{\lambda}{2\pi}\right)^{\frac{2}{5}}(C_n^2)^{\frac{6}{5}}(R_1)^{\frac{16}{5}}}{R_1}\right)^2\right)}-\frac{(y-u_{BS})^2}{2R_1^2\left(\delta_b^2+\delta_j^2+\left(\frac{3.98\left(\frac{\lambda}{2\pi}\right)^{\frac{2}{5}}(C_n^2)^{\frac{6}{5}}(R_1)^{\frac{16}{5}}}{R_1}\right)^2\right)}\right)}{2\pi R_1\sqrt{\delta_b^2+\delta_j^2+\left(\frac{3.98\left(\frac{\lambda}{2\pi}\right)^{\frac{2}{5}}(C_n^2)^{\frac{6}{5}}(R_1)^{\frac{16}{5}}}{R_1}\right)^2}}dxdy\left(e^{-\alpha_2 R_2}\right)\left(\frac{\pi\left(\frac{D_{Rx}}{2}\right)^2}{\pi R_2^2}\right)\tau_{Rx} \quad (4)$$

where E_{Pulse} is the energy per laser pulse, $\triangle t$ is the laser pulse width, τ_{Tx} is the transmissivity of the laser designator, α_1 is the atmospheric air's extinction coefficient between the laser designator and the target, R_1 is the distance between the laser designator and the target, ρ is the target's reflectivity, θ is the angle between the laser designator and the camera, H is the height of the footprint, W is the width of the footprint, u_{BS} is the bore-sight error, α_2 is the atmospheric air's extinction coefficient between the target and the receiving part, R_2 is the distance between the target and the receiving part, D_{Rx} is the diameter of the entrance pupil of the receiving part's optical system, τ_{Rx} is the transmissivity of the receiving part's optical system, δ_b is the laser beam's divergence angle, δ_j is the jitter of the laser designator, λ is the laser's wavelength, and C_n^2 is the refractive-index structure function.

Table 2 shows the parameters used for calculating the detection range of the LADAR sensor. For the laser designator, a laser with 1540 nm wavelength was selected, considering laser eye safety. The laser beam's divergence angle was set to 4°, identical to the field of view of the optical system. It was assumed that there is no alignment error between the laser designator and the camera. The jitter of the laser designator was set to 50 μrad, which is a general value. The atmospheric air's extinction coefficient of 0.057 km^{-1} is a value corresponding to a visibility of 15 km, derived using the commercial software PcModwin 4.0. The refractive-index structure function was set to 5×10^{-15} $m^{-2/3}$, as shown in Fig. 1. The target's size is identical to the laser beam's size at a point 1000 m from the laser designator, and this indicates that the transverse mode of the laser beam is square. The target's reflectivity was set to 30%, which is a general condition. The laser designator and camera were assumed to have been installed in the same equipment, and the LOS (line of sight) angle was set to 0°. The distance between the laser designator and the target of the LADAR sensor was set to 1000 m or less. To analyze the quantity of light received according to the diameter of the entrance pupil, the quantity of light was calculated for entrance pupils with diameters of 5, 7, 10, 12, and 15 cm. The laser designator and camera were assumed to have no optical loss.

Figure 2 shows the quantity of laser light received per pixel of the LADAR sensor, according to the entrance-pupil diameter of the optical system in relation to the distance. The calculation was conducted using Eq. (4) and the

TABLE 2. Detection-range calculation parameters

Description	Symbol	Units	Value
Laser energy per pulse	E_{Pulse}	mJ	10
Laser pulse width	$\triangle t$	ns	5
Laser efficiency	τ_{Tx}	-	1
Laser wavelength	λ	nm	1540
Intrinsic beam divergence, x-direction	δ_b	degrees	4
Boresight error at target	u_{BS}	mrad	0
Stabilization divergence	δ_j	mrad	50
Extinction coefficient, transmitter to target	α_1	km^{-1}	0.057
Extinction coefficient, target to receiver	α_2	km^{-1}	0.057
Refractive index structure constant	C_n^2	$m^{-2/3}$	5×10^{-15}
Footprint height	H	m	63
Footprint width	W	m	63
Target hemispherical reflectivity	ρ	-	0.3
Angle, Target normal to receiver LOS	θ	degrees	0
Range, Transmitter to target	R_1	m	200-1000
Range, Target to receiver	R_2	m	200-1000
Entrance pupil diameter, receiver optics	D_{Rx}	cm	5-20
Receiver efficiency	τ_{Rx}	-	1

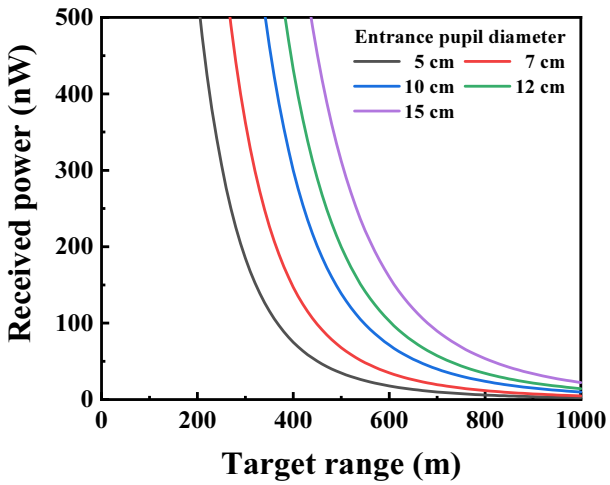

FIG. 2. The quantity of laser light received per pixel of the LADAR detector, as a function of target range, for several diameters of the entrance pupil of the optical system.

parameter values shown in Table 2. The received quantity of laser light shows a tendency to decrease as the target range increases, and at a given distance, a larger quantity of laser light is received when the diameter of the entrance pupil is larger. At the maximum detection range of 1000 m, when the diameter of the entrance pupil was 5, 7, 10, 12, and 15 cm, the quantity of light received per pixel of the LADAR detector was calculated as 2.5, 4.8, 9.9, 14.2, and 22.3 nW respectively. The target can be detected even when diameter of the entrance pupil is 15 cm, because the quantity of light received is larger than the minimum detectable signal of 20.5 nW. However, for the diameter of the entrance pupil, atmospheric air attenuation under various conditions should be considered.

Figure 3 shows the quantity of laser light received per pixel of the LADAR detector versus the diameter of the entrance pupil, for different atmospheric extinction coefficients. The calculation was conducted using Eq. (4) and the parameter values shown in Table 2. The received quantity of laser light shows a tendency to increase as the diameter of the entrance pupil's target range becomes larger, and at a given diameter of the entrance pupil, a larger quantity of light of laser is received when the atmospheric air's extinction coefficient is smaller. According to the results of the LADAR detector analysis, when the SNR is not smaller than 5, laser signals can be detected in cases where the quantity of laser light received is at least 20.5 nW. In cases where the diameter of the entrance pupil was 15.7 cm, when the atmospheric air's extinction coefficient value was 0.140, 0.081, and 0.039 km^{-1}, the quantity of light received per pixel of the LADAR detector was calculated as 20.7, 23.3, and 25.3 nW respectively. The analysis indicates that to obtain detection ranges not shorter than 1000 m, the diameter of the entrance pupil should be at least 15.7 cm, regardless of the atmospheric air's extinction coefficient. The diameters of the entrance pupil shown in Fig. 3 are applied when the common optical system is designed, which will be explained in the

following chapter.

Figure 4 shows the pointing error versus target range, according to refractive-index structure. Pointing errors are caused by laser-beam divergence angles, laser-beam jitter, and refractive-index structure. Although the laser-beam divergence angles and jitter are output-power characteristics of the laser light source, the refractive-index structure differs depending on the ambient conditions. The laser pointing error was calculated using Eq. (4). At the target range of 1000 m, when the refractive-index structure increases to 1×10^{-15}, 5×10^{-15}, 1×10^{-14} and 5×10^{-14} $m^{-2/3}$, the pointing error also increases to 3.9, 10.3, 15.7, and 41.1 μrad respectively. That is, at the target range of 1000 m, the laser beam irradiated to the target varies by 4.1 cm at most, because of the beam-wander effect. In the case where the field of view of the optical system is assumed to be 4 degrees and the measurement resolution for 1 pixel of the LADAR detector is assumed to be 54.6 cm at the target range of 1,000 m, the laser pointing error due to refractive-index structure is identified to be 7.5%.

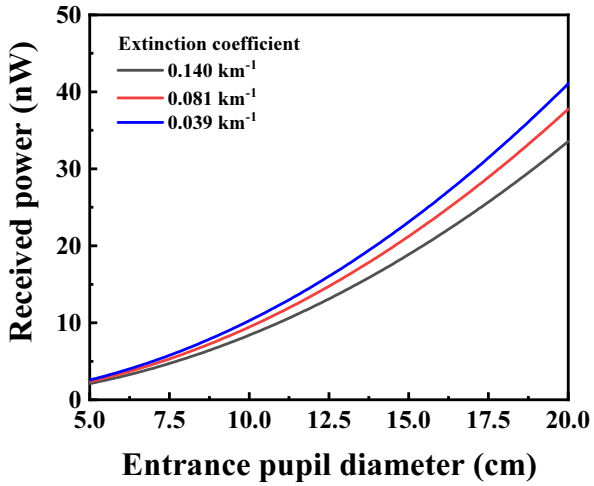

FIG. 3. The quantity of laser light received per pixel of the LADAR detector, as a function of diameter of the entrance pupil, for several extinction coefficients.

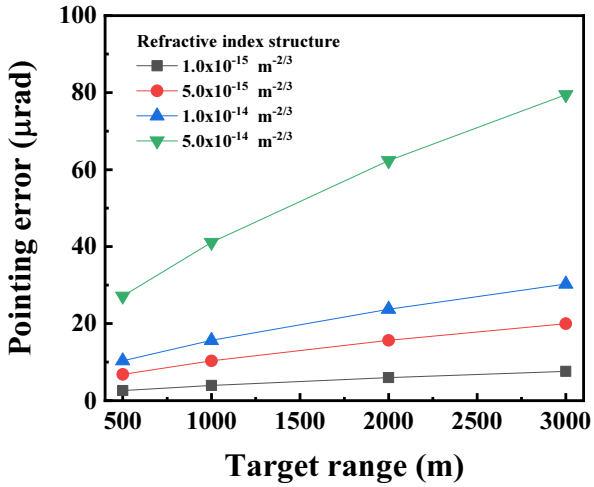

FIG. 4. Turbulence contributions to target range, according to refractive-index structure function.

IV. DESIGN OF A COMMON OPTICAL SYSTEM

Figure 5 shows the ray tracing and layout of the designed common optical system. The common optical system was composed of a LADAR optical system and a LWIR optical system, to receive the energy reflected and radiated by the target. The energy of the target enters the optical system through the common lens group, and is split into the LADAR wavelength band (1.54 μm) and the LWIR wavelength band (7.75~12.77 μm) by the beam splitter. The LADAR wavelength band penetrates the beam splitter to progress, and is concentrated on the LADAR sensor face through the LADAR lens group. The LWIR wavelength band was designed to be reflected by the beam splitter and concentrated on the LWIR sensor face through the LWIR lens group. From the results of the detection-range analysis, the diameter of the entrance pupil of the LADAR optical system was designed as 15.7 cm, and at a target range of 1000 m the ground spot diameter is 69.81 × 69.81 m. The optical system's design specification

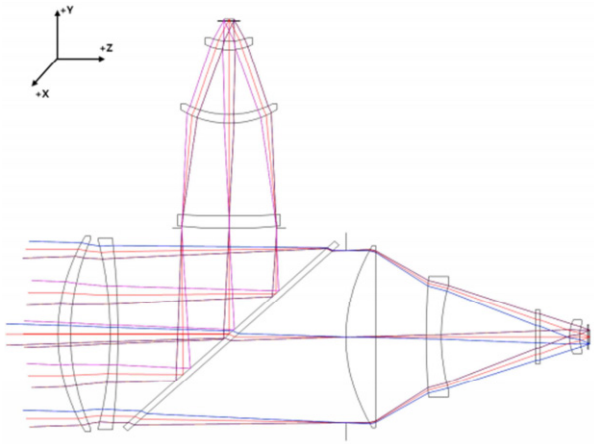

FIG. 5. Ray tracing and layout of the designed common optical system.

TABLE 3. Optical system design specification

Parameter	Units	LADAR	LWIR
Spectral range	μm	1.54	7.75-12.77
Effective focal length	mm	183.3	93.1
F-number	-	1.17	1.20
Entrance pupil diameter	mm	157	77.6
Field of view (H × V)	degrees	4.0 × 4.0	6.7 × 5.0
Pixel format	pixels	128 × 128	640 × 480
Pitch	μm	100	17.0

is provided in Table 3.

Table 4 shows the lens data for the LADAR optical system. Table 5 shows the lens data for the LWIR optical system. For the common lens group, zinc sulfide was selected as the lens material, so that the LADAR and LWIR wavelength band energies would penetrate simultaneously. The common lens group consists of two ZnS lenses. The first lens was selected to have positive refractive power, while the second lens was selected to have negative refractive power. To minimize sensitivity to fabrication and assembly, all of the common lenses were made to have spherical surfaces, rather than aspherical. The beam splitter plays the role of allowing the LWIR wavelength band to penetrate, while reflecting the LADAR band. The transmission and reflection performances could be optimized through multilayer-thin-film technology. The beam splitter is tilted 45 degrees to reflect the LADAR energy. The LADAR lens group plays the role of minimizing the residual aberration of the rays that have penetrated through

TABLE 4. LADAR optical system lens data

Surface	Radius (mm)	Thickness (mm)	Material
1. Common Lens#1	195.09	10.0	ZnS
2. Common Lens#1	239.92	32.0	Air
3. Common Lens#2	-388.74	6.5.0	ZnS
4. Common Lens#2	-847.50	90.0	Air
5. Beam Splitter (45° Tilt)	-	5.0	ZnS
6. Beam Splitter	-	90.0	Air
7. Stop	-	-	Air
8. LADAR Lens#1 (ASP)	165.08	24.10	ZnS
9. LADAR Lens #1	-	41.29	Air
10. LADAR Lens#2	834.84	12.20	ZnS
11. LADAR Lens#2 (ASP)	207.84	76.68	Air
12. Bandpass Filter	-	3.00	ZnS
13. Bandpass Filter	-	24.29	Air
14. LADAR Lens#3	40.60	8.00	ZnS
15. LADAR Lens#3	38.02	6.50	Air
16. Detecting Window	-	1.00	NBK7
17. Detecting Window	-	1.00	Air
18. Image	-	-	-

TABLE 5. LWIR optical system lens data

Surface	Radius (mm)	Thickness (mm)	Material
1. Common Lens#1	195.09	10.0	ZnS
2. Common Lens#1	239.92	32.0	Air
3. Common Lens#2	-388.74	6.5.0	ZnS
4. Common Lens#2	-847.50	90.0	Air
5. Beam Splitter (Reflect)	-	-97.0	ZnS
6. Stop	-	-	Air
7. LWIR Lens#1	-343.40	-12.0	Ge
8. LWIR Lens#1	-462.19	-85.0	Air
9. LWIR Lens#2 (ASP)	-66.27	-8.0	Ge
10. LWIR Lens#2	-70.69	-59.28	Air
11. LWIR Lens#3	-40.41	-8.00	Ge
12. LWIR Lens#3	-38.55	-17.92	Air
13. Detecting Window	-	-0.76	Ge
14. Detecting Window	-	-1.09	Air
16. Image	-	-	-

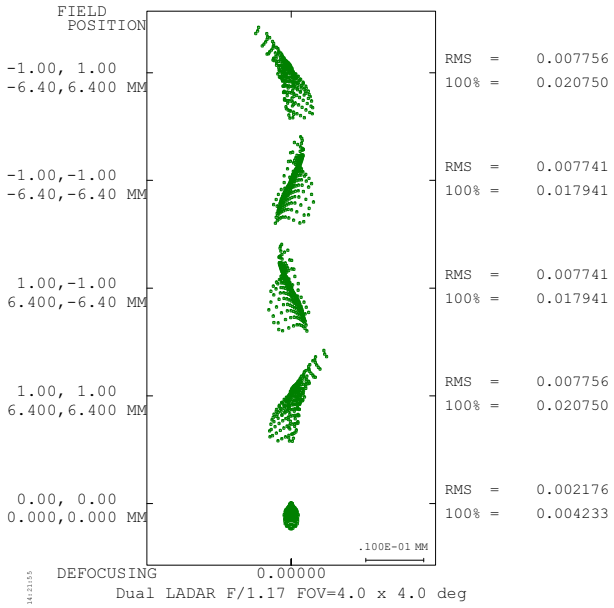

(a)

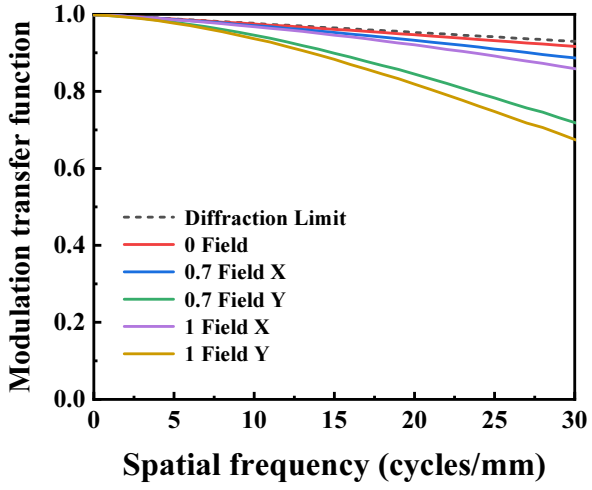

(b)

FIG. 6. (a) Spot diagrams and (b) MTFs of the LADAR optical system, according to the field.

the common optical system. This lens group was composed of three ZnS lenses and a band-pass filter, and included one or more aspherical surfaces. For the band-pass filter, a half-width of 100 nm was selected to obtain high transmissivity. The LWIR lens group was also composed of three germanium lenses, to minimize the residual aberrations of the rays that have penetrated through the common optical system, and it included one aspherical surface.

Figure 6 shows the results of the spot diagram and MTF analysis by field, conducted through LADAR optical system ray tracing. The spot diagram in Fig. 6(a) shows that the root-mean-square (RMS) geometric spot size is 2.2 μm and the total geometric spot size is 4.2 μm, based on zero field; this indicates that the pitch of 1 pixel is 100 μm or less. As shown in Fig. 6(b), the MTF of all fields is 98.8% of the MTF of the diffraction limit, at the spatial frequency of 5 cycles per millimeter.

Figure 7 shows the results of analyses of the spot diagrams and MTFs of the LWIR optical system. The spot diagram in Fig. 7(a) shows that the RMS geometric spot size is 9.4 μm and the total geometric spot size is 16.6 μm, based on zero field; this indicates that the pitch of 1 pixel is 17 μm or less. As shown in Fig. 7(b), the MTF of all fields is 92.4% of the MTF of the diffraction limit, at the spatial frequency of 29 cycles per millimeter.

Figure 8 shows the probabilities of detection, recognition, and identification by the LWIR optical system, according to distance. To analyze the detection performance of the designed LWIR, the commercial software Night Vision Thermal Imaging Systems Performance Model (NVTherm

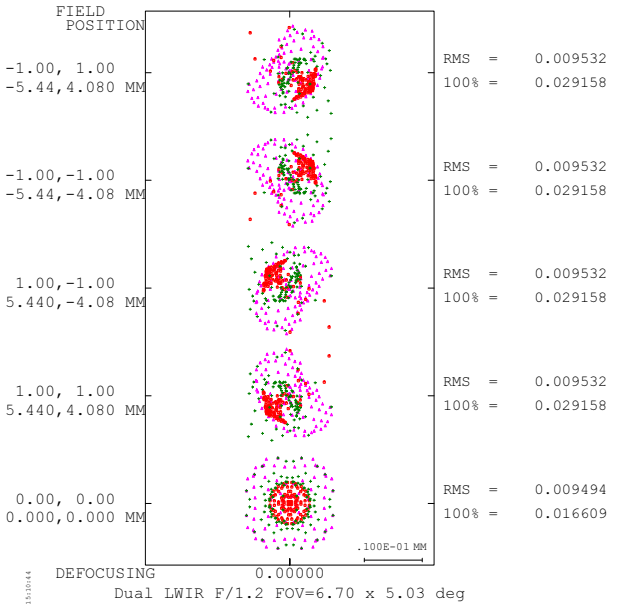

(a)

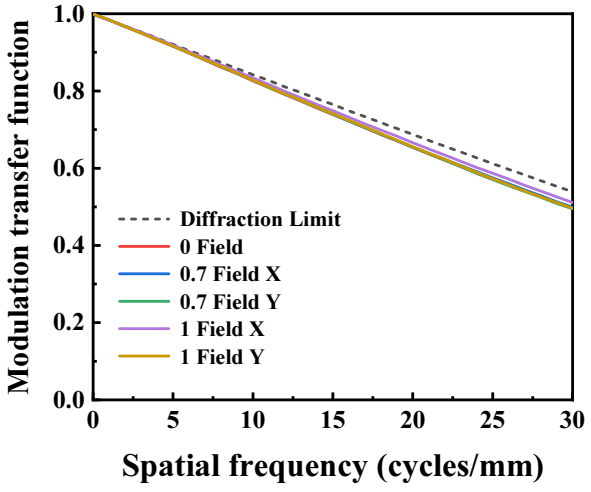

(b)

FIG. 7. (a) Spot diagrams and (b) MTFs of the LWIR optical system, according to the field.

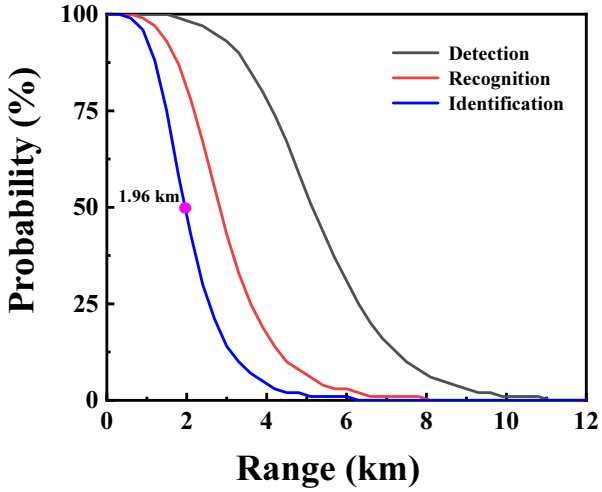

FIG. 8. Probabilities of detection, recognition, and identification for the LWIR optical system, according to distance.

TABLE 6. Parameters for LWIR optical system detection-range analysis

Parameter		Unit	Value
Optics	Transmission	-	0.65
	F/#	-	1.20
Detector	Peak D*	cm $\sqrt{Hz}$ /W	4.46×10^{8}
	Integration time	ms	20
	Noise	K	0.11
	Frame rate	Hz	50
Atmo-sphere	Transmission per kilometer	-	0.77
	Turbulence	$m^{-2/3}$	5.00×10^{-15}
Target	Target contrast	delta celsius	2
	Size	m	6.5 × 6.5
	Detection Recognition Identification	cycles	3 6 9

2002) was used; Table 6 shows the parameters used in the performance analysis. The optical system's parameters are reflected in the LWIR optical system's design specification. The transmissivity values for one lens, the beam splitter, and the detector window were calculated as 97%, 80%, and 95% respectively. For the detector, the specification of a commercial detector with 640 × 480 pixels was reflected. The atmospheric air's transmissivity was calculated on the basis of 15 km of visibility under good weather conditions, and atmospheric turbulence was assumed to be moderate. The temperature difference between target and background is 2 K, and the target size is 6.5 × 6.5 m. The criteria for detection, recognition, and identification according to distance were set to 3, 6, and 9 cycles. Analysis of the LWIR optical system as a function of distance showed that the detection range is 5.14 km, recognition distance is 2.82 km, identification distance is 1.96 km, based on a probability of 50%.

V. CONCLUSION

In the present study, a common optical system was investigated for the acquisition and fusion of 3D LADAR images together with infrared-camera images. The refractive-index structure has been observed to have larger beam-wander effects as the altitude decreases, and the maximum beam-wander effect of 2.54×10^{-15} $m^{-2/3}$ was identified at an altitude of 200 m. An analysis of the pointing error by refractive-index structure of the target range revealed that the maximum variation is 4.1 cm at a target range of 1000 m. An array detector using 128 × 128-pixel linear-mode avalanche photodiodes capable of implementing large-area images was analyzed. The minimum detectable signal necessary for the LADAR system to stably detect the laser signal reflected from the target was calculated to be 20.5 nW. Analysis of the detection range of the LADAR sensor revealed that the diameter of the entrance pupil should be greater than 15.7 cm to detect the target at a range of 1000 m, regardless of the atmospheric air attenuation. A common optical system using LADAR sensors and LWIR sensors was designed and analyzed. For the LADAR optical system, the MTF of all fields was shown to be 98.8% at a spatial frequency of 5 cycles per millimeter. For the LWIR optical system, the MTF of all the fields was shown to be 92.4% at a spatial frequency of 29 cycles per millimeter. The detection, recognition, and identification distances of the LWIR optical system were found to be 5.14, 2.82, and 1.96 km respectively, at a probability of 50%. In the future, the optical system using LADAR sensors and LWIR sensors will be useful for the take-off and landing of drones or unmanned air vehicles, and can be used to prevent the collision of helicopters or drones.

REFERENCES

1. M. Henriksson, "Detection probabilities for photon-counting avalanche photodiodes applied to a laser radar system," Appl. Opt. **44**, 5140-5147 (2005).
2. R. D. Richmond, R. Stettner, and J. W. Glessner, "Eye-safe laser radar focal plane array for three-dimensional imaging," Proc. SPIE **4035**, 172-179 (2000).
3. M. J. Halmos, M. D. Jack, J. F. Asbrock, C. Anderson, S. L. Bailey, G. Chapman, E. Gordon, P. E. Herning, M. H. Kalisher, L. F. Klaras, K. Kosai, V. Liquori, M. Pines, V. Randall, R. Reeder, J. P. Rosbeck, S. Sen, P. A. Trotta, P. Wetzel, A. T. Hunter, J. E. Jensen, T. J. DeLyon, C. W. Trussell, J. A. Hutchinson, R. S. Balcerak, "3-D flash ladar at Raytheon," Proc. SPIE **4377**, 84-98 (2001).
4. C.-I Chen and R. Stettner, "Drogue tracking using 3D flash lidar for autonomous aerial refueling," Proc. SPIE **8037**, 80370Q (2011).
5. M. S. Baran, R. L. Tutwiler, D. L. Hall, and D. J. Natale, "3DSF: three-dimensional spatiotemporal fusion," Proc. SPIE **8062**, 80620E (2011).
6. D. A. Fay, J. G. Verly, M. I. Braun, C. Frost, J. P. Racamato, and A. M. Waxman, "Fusion of multi-sensor passive and active 3D imagery," Proc. SPIE **4363**, 219-230 (2001).
7. R. Q. Fugate, *Handbook of Optics* (McGraw-Hill, Volume V, 2010).
8. D. Winker, "Unpublished air force weapons lab memo, 1986," U.S. Airforce (1986).
9. L. C. Andrews and R. L. Phillips, "Laser beam propagation through random media," SPIE Press **482** (2005).
10. J. C. Rock, J. Mullins, and P. Ruffin, "Prospects on low-cost phased arrays using RF and optical MEMS," in *Proc. IEEE Aerospace Conference Proceedings* (USA, Mar. 2004), pp. 930-939.
11. O. Steinvall, T. Carlsson, C. Gronwall, H. Larsson, P. Andersson, and L. Klasen, "Laser based 3D imaging new capabilities for optical sensing," Swedish Defense Research Agency (2003).
12. G. C. Holst, *Holst's Practical Guide to Electro-optical Systems* (JCD Publishing, 220, 2013).
13. P. F. McManamon, P. S. Banks, J. D. Beck, D. G. Fried, A. S. Huntington, and E. A. Watson, "Comparison of flash lidar detector options," Opt. Eng. **56**, 031223 (2017).
14. S. Kim, I. Lee, and Y. Lee, "Simulation and performance assessment of a geiger-mode imaging LADAR system," J. KIMST **15**, 687-698 (2012).
15. M. Friedman, J. Hixson, and Q. Nguyen, *The Night Vision Laser Designator NVLaserD Users Manual* (U. S. ARMY RDECOM, CERDEC, Night Vision and Electronic Sensors Directorate Modeling and Simulation Division, 2006).